ACS NANO

www.acsnano.org

ARTICLE

Halogen Etch of Ti_3AlC_2 MAX Phase for MXene Fabrication

Ali Jawaid,[⊥] Asra Hassan,[⊥] Gregory Neher, Dhriti Nepal, Ruth Pachter, W. Joshua Kennedy, Subramanian Ramakrishnan, and Richard A. Vaia*

Cite This: *ACS Nano* 2021, 15, 2771–2777

Read Online

ACCESS | Metrics & More | Article Recommendations | Supporting Information

ABSTRACT: **The versatile property suite of two-dimensional MXenes is driving interest in various applications, including energy storage, electromagnetic shielding, and conductive coatings. Conventionally, MXenes are synthesized by a wet-chemical etching of the parent MAX-phase in HF-containing media. The acute toxicity of HF hinders scale-up, and competing surface hydrolysis challenges control of surface composition and grafting methods. Herein, we present an efficient, room-temperature etching method that utilizes halogens (Br_2, I_2, ICl, IBr) in anhydrous media to synthesize MXenes from Ti_3AlC_2. A radical-mediated process depends strongly on the molar ratio of the halogen to MAX phase, absolute concentration of the halogen, the solvent, and temperature. This etching method provides opportunities for controlled surface chemistries to modulate MXene properties.**

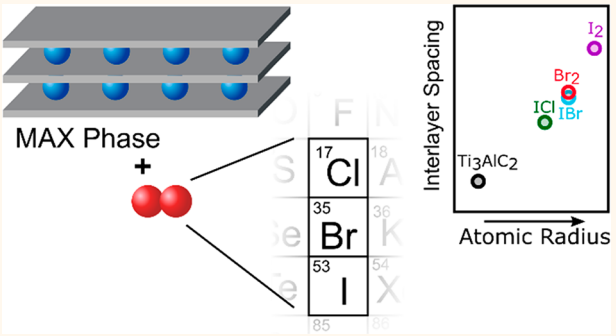

KEYWORDS: *2D materials, transition-metal carbide, MXene, synthesis, halogen etching*

Layered transition-metal carbides and carbonitrides, also known as MXenes, offer a combination of high electrical conductivity and excellent mechanical properties, which are rarely seen in other two-dimensional (2D) crystals, such as element-enes (*e.g.*, phosphene), transition-metal dichalcogenides (TMDs), phyllosilicates (nanoclays), *etc.*[1−4] MXenes are described by a general chemical formula of $M_{n+1}X_nT_x$ (n = 1−4), where M represents an early transition metal, X is carbon and/or nitrogen, and T_x represents the surface terminations.[4−6] They are produced by the selective etching of the A interlayer from their parent three-dimensional (3D) MAX phase ($M_{n+1}AX_n$).[7] Delamination and incorporation of the MXene layers into composites, inks, and films have attracted considerable attention in conductive coatings, optoelectronics, catalysis, and energy storage.[8−12]

State-of-the-art etching utilizes HF-containing media such as *in situ* generation of HF via salts or acids (LiF/HCl,[13] $NaHF_2$, KHF_2, NH_4HF_2[14]). A mixture of MAX powders and etchant produces a clay-like precipitate, which upon postprocessing (aqueous washing, intercalation, and mechanical agitation) yields a distribution of MXene morphologies. However, HF-containing waste is highly toxic and corrosive. Additionally, MXenes, such as $Ti_3C_2T_x$, are hydrolytically unstable, and thus the quality and yield vary significantly.[15] Furthermore, the MXene surface is compositionally heterogeneous, containing fluoro, oxo, and hydroxyl terminations. Properties, such as optical, electronic, and chemical performance, are highly sensitive to the surface structure and composition resulting in suboptimal performance, such as for supercapacitors or electromagnetic coatings.[4,10,22−24,16−22,25,26] Solid-state methods such as molten salt etching[27,28] have been developed as an attempt to mitigate aqueous HF approaches; however, they require high temperatures (550 °C), limiting many utilizations.

Safe, efficient formation of MXenes with a broad range of homogeneous surfaces thus remains an experimental challenge. To this end, we discuss a room-temperature (RT) etching method to remove the A-layer using elemental halogen and interhalogen compounds to produce exfoliated MXenes with homogeneous Cl, Br, or I surfaces.[29] All chemical processes involving the use of halogens are optimized and performed in a safe and controllable manner in an isolated glovebox. Hazardous byproducts are readily quenched by adding a stabilizing agent avoiding any undesired exposures and significantly enhancing the process safety. Safe handling

Received: October 15, 2020
Accepted: January 21, 2021
Published: January 27, 2021

https://dx.doi.org/10.1021/acsnano.0c08630
ACS Nano 2021, 15, 2771–2777

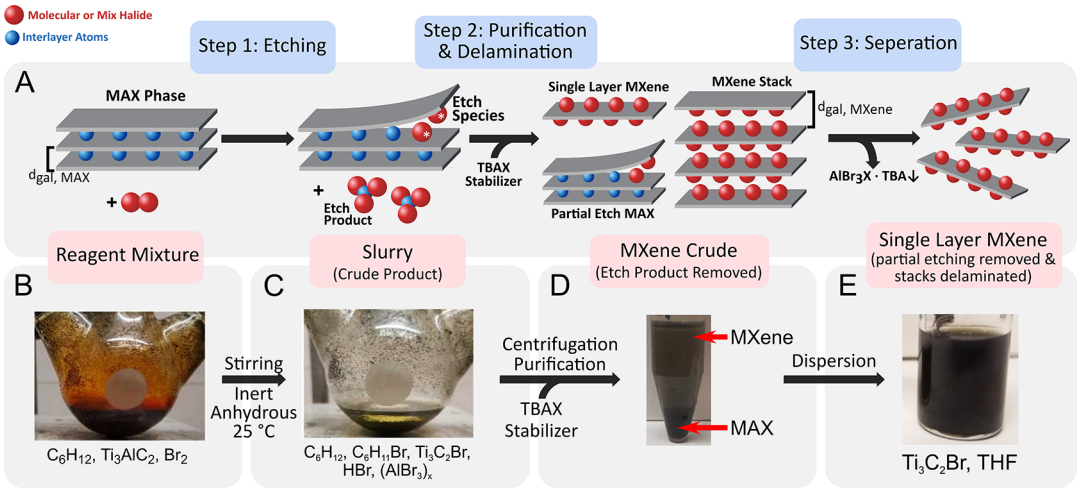

Figure 1. Halogen etch of MAX phases. (A) Generalized process for the formation of delaminated, halogen-terminated MXenes. (B) Addition of Br_2 to Ti_3AlC_2 in anhydrous cyclohexane produces a deep red solution. (C) As Br_2 reacts with the Al interlayer, the supernatant turns to a pale yellow color, reflecting a depletion of Br_2 and the production of $AlBr_3$ species. $AlBr_3$ is rendered inert by addition of stabilizers (tetrabutylammonium bromide, TBAX). (D) The MXene crude is purified via repeated redispersion in nonpolar solvent (*i.e.*, $CHCl_3$). (E) The purified size-selected MXene is obtained via centrifugation and dispersed in THF.

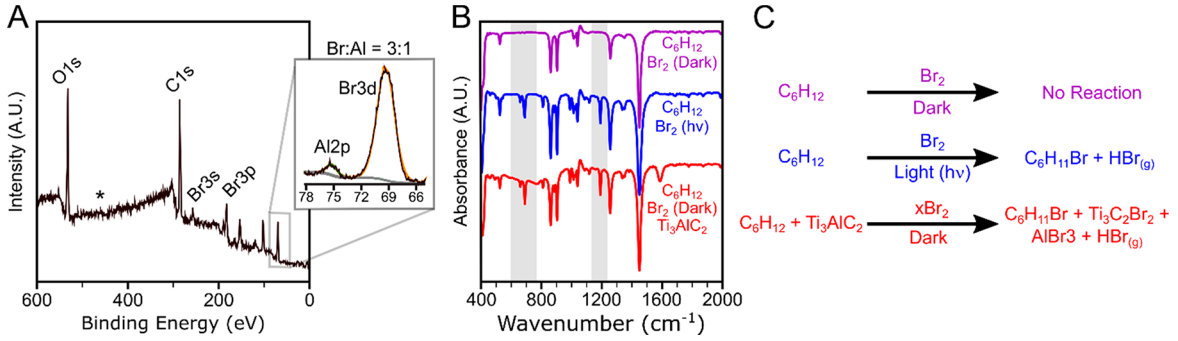

Figure 2. Etched products in the Ti_3AlC_2/Br_2supernatant. (A) XPS survey spectrum of Br and Al indicate a 3:1 stoichiometry ($AlBr_3$). The absence of Ti-2p (454−465 eV) confirms selective etching of the A layer. (B) FTIR spectra of the supernatant (red) in comparison to UV-activated Br* halogenation of cyclohexane (blue) and unreactive cyclohexane−Br_2 mixture (purple). Absorption peaks attributed to $C_6H_{11}Br$ are highlighted. (C) A summary of the reactions leading to the spectra in B.

procedures are outlined in the Supporting Information. In parallel to the work discussed herein, high-temperature molten-salt approaches for MXenes production have very recently been reported that likely rely on similar mechanisms of an *in situ* production of halogen radicals.[30]

Halogen-based etching (*e.g.*, molecular chlorine, bromine, and iodine) is broadly used in manufacturing, including the fabrication of semiconductor devices, where their high etch rates have enabled nanofabrication since the 1980s.[31−33] A species-specific etch method must simultaneously balance (a) solubility of reactants in an inert medium, (b) formation of bound site-specific etch precursors, (c) reaction kinetics favoring liberation of a stable etch product that exposes sites for subsequent reactions, and (d) facile separation of these etch products to yield a purified final product. As an exemplar of halogen-based MXene production from Ti_3AlC_2, Figure 1A summarizes these criteria for the production of colloidally stable, layered $Ti_3C_2T_x$ (T_x = Br) using Br_2 to etch Ti_3AlC_2 in anhydrous cyclohexane (CH) with tetrabutyl ammonium bromide to stabilize etch byproducts.

RESULTS AND DISCUSSION

Because of the high reactivity of elemental halogens with Al,[34] introduction of Br_2 to Al-containing materials produces $(AlBr_3)_x$,[35−37] where the x-mer dissociates readily into monomeric $AlBr_3$. For example, an initial deep red mixture (Figure 1B) of Ti_3AlC_2 powder (1.0 mmol) suspended in a 2.0 M solution of bromine in cyclohexane (CH) changes to light yellow over 24 h at RT and inert atmosphere, indicating consumption of the reddish-brown Br_2 and production of pale yellow $AlBr_3$ (Figure 1C). $AlBr_3$'s high solubility in nonpolar solvents[38−40] provides strong driving force for a selective removal of etched Al from the MAX phase surface. The synthetic details are summarized in the Experimental Section. X-ray diffraction (XRD, Figure S1) spectra of the crude media indicate an interlayer expansion (8.8°) and production of an etched product (ca. 20°−30°). X-ray photoelectron spectroscopy (XPS) analysis (Figure 2A) of the yellow supernatant resolves only Al and Br (1:3 stoichiometric ratio) with no Ti—confirming selective etching at these conditions. A white precipitate (Al_2O_3) forms upon exposure of the supernatant to air, consistent with hydrolysis of the highly reactive $(AlBr_3)_x$[41] (Figure S2). Fourier-transform infrared spectroscopy (FTIR) analysis of the yellow supernatant reveals brominated cyclo-

https://dx.doi.org/10.1021/acsnano.0c08630
ACS Nano 2021, 15, 2771−2777

hexane ($C_6H_{11}Br$); see the Experimental Section for further details. Bromination of aliphatic solvents occurs via free-radical processes, which typically require either catalytic or photonic activation of Br_2 homolysis, and produces HBr gas.[42,43] Figure 2B demonstrates CH/Br_2 halogenation in the presence of UV light (354 nm). Etch solutions run in the dark, however, also produce $C_6H_{11}Br$ and HBr, which strongly suggests that Ti_3AlC_2 surfaces act as catalysis sites for Br_2 homolysis.

These observations are consistent with a bromine radical etch of Ti_3AlC_2. Initially, Br_2 adsorption to exposed edges of the Al plane likely induce Br_2 homolysis at the surface. The generated radicals react with Al centers and solvent, accounting for all etched products observed (HBr, $AlBr_3$, $C_6H_{11}Br$). This mechanism can be further confirmed via consideration of MAX phase etching in different solvents. We found that surface Br−Br dissociation is solvent-dielectric-dependent. High-dielectric solvents increase the reactivity of Br_2 after surface adsorption through solvent coordination, which expands the type of surface sites that may produce radicals (Br*), thus lowering selectivity. Figure S3 and Table S1 confirm this trend, where Br_2 in high-dielectric solvents, such as acetonitrile, react violently with Ti_3AlC_2 and result in $TiBr_x$ formation. Thus, selectivity is enhanced in nonpolar solvents, such as CH. We speculate that a similar halogen radical mechanism drives recently reported molten salt preparations, where thermal decompositions of transition-metal halide salts are known to result in the formation of zerovalent transition metals and elemental halogens.[30,44]

Consistent with this mechanistic insight, the most effective etching conditions (rate and specificity) occur at intermediate Br_2 concentrations in cyclohexane. This is analogous to the parabolic concentration profile of silicon etching via Br_2 and Cl_2 at RT.[45,46] For example, etching is optimized at ∼10 vol % Br_2 using a slightly depleted stoichiometric molar ratio of MAX/Br_2 of 1:2 (Al/Br = 1:4) relative to the $Ti_3C_2Br_2$ and $AlBr_3$ products (Figure 2C). Lowering the Br_2 concentrations (0.1−1 vol %) reduces the etch rate (Figure S4), due to lower local areal concentrations of Br_2 adsorbates. Conversely, increasing the Br_2 concentration reduces the effectiveness of the etch (Figure S5). This is likely due to an increase of reactive species at the surface (*e.g.*, Br* and $AlBr_3$) that reduces specificity *via* side reactions. For example, titanium bromides and amorphous carbon are formed at greater than 10 vol % Br_2, and Ti_3AlC_2 reacts violently upon its addition to neat Br_2, yielding carbonaceous species (Figure S6). These observations are consistent with prior reports of carbon-derived carbide (CDC) synthesis *via* etching of metalloid atoms (Ti, Si, *etc.*) from binary or ternary carbides *via* halogenation.[47]

Purification and isolation of $Ti_3C_2Br_x$ flakes (Figure 1D) require removal of $AlBr_3$ while inhibiting its spontaneous hydrolysis to aluminum oxides.[41] Formation of Al_2O_3 on Ti_3AlC_2 and $Ti_3C_2T_x$ surfaces reduces the etch rate and confounds purification. The former is similar to processes where an Al_2O_3 layer is employed to protect Al from Cl_2, Br_2, or glow discharge of these vapors.[41,48,49] $AlBr_3$ cannot be volatilized at RT (boiling point (BP) 263 °C); however, it can be stabilized by complexation with an anion to form an inert, soluble, tetragonal $[AlBr_3X]^-R^+$ species (Figure S7).[50,51] Tetrabutylammonium halides (TBA^+X^-; X^- = F^-, Cl^-, Br^-, I^-) do not interfere with Br* generation and can be added before or after the etch, yielding pristine, high-quality MXenes that are isolated by standard centrifugation separation in ambient conditions (Figure 1E; see the Experimental Section for the processing and cleaning procedure). Solutions obtained from these washing procedures result in highly colloidally stable materials (more than two weeks).

Figure 3 summarizes the final $Ti_3C_2Br_x$ MXene. XRD patterns indicate that the etched crude solution (Figure 3A, magenta curve) contains a mixture of unetched Ti_3AlC_2 powder (9.55°), $Ti_3C_2Br_x$, (8.8°), and byproducts such as Al_2O_3 and $(AlBr_3)_x$ (ca. 20−30°). After addition of TBAX and purification (centrifugation), only $Ti_3C_2Br_x$ is present (Figure 3A, red curve). The expansion of the $Ti_3C_2Br_x$ unit cell (d(002) Ti_3AlC_2 = 0.927 nm; d(002) $Ti_3C_2Br_x$ = 1.01 nm) is consistent with recent reports of $Ti_3C_2Br_x$ from molten $CdBr_2$.[30] Transmission electron microscopy (TEM) images show thin, two-dimensional flakes with minimal surface contamination (Figure 3B). The in-plane single-crystal morphology is preserved ((200) = 0.35 nm), indicating that the structural integrity of the Ti−C backbone of the MXene is not damaged during the etching process. Compositional analysis of the purified MXene is consistent with halogenated surfaces (Figure 3C−E, Tables S2 and S3), with a Ti/Br composition of ∼3:1, similar to molten salt approaches (ca. 3:1.5).[30] Atomic force microscopy (AFM) indicates ∼2−3 nm thick sheets (Figure S9), where surface adsorbates typically increase observed monolayer heights, as previously reported for other 2D systems.[52−54]

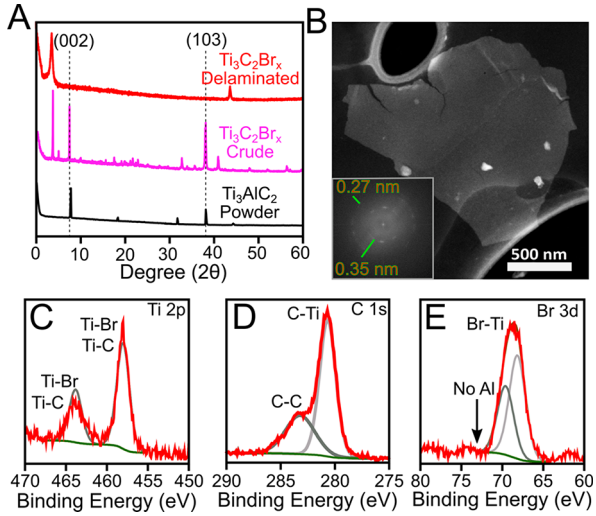

Figure 3. Structure and composition of $Ti_3C_2Br_x$. (A) XRD patterns of bulk Ti_3AlC_2 (black) and resulting crude (magenta) and purified (red) $Ti_3C_2Br_x$ synthesized with 10% Br_2/CH. The addition of TBAB to the crude enables separation of dispersed $Ti_3C_2Br_x$ flakes from the etch byproducts. (B) STEM image of a purified, exfoliated $Ti_3C_2Br_x$ MXene flake (inset, FFT of an HRTEM image (Figure S8) reveals (110) (0.35 nm) and (200) (0.27 nm) lattice reflections. (C−E) High-resolution XPS spectra of purified $Ti_3C_2Br_x$ flakes showing titanium (Ti 2p 454 eV), carbide (C 1s 281.5 eV), Ti−Br (66−69 eV), and absence of Al (72−75 eV).

Halogen-based production of MXene extends beyond Br_2, due to the generality of the halogen radical etch of metals and their alloys;[40,45] Figure 4 summarizes the results using I_2 as well as interhalogen etchants (ICl, IBr) (the procedures are summarized in the Experimental Section). For example, reactions utilizing I_2 are initially deep purple and slowly turn light purple to colorless as the Al is removed. Due to iodine's larger atomic radius and endothermic homolysis relative to Br_2,

https://dx.doi.org/10.1021/acsnano.0c08630
ACS Nano 2021, 15, 2771−2777

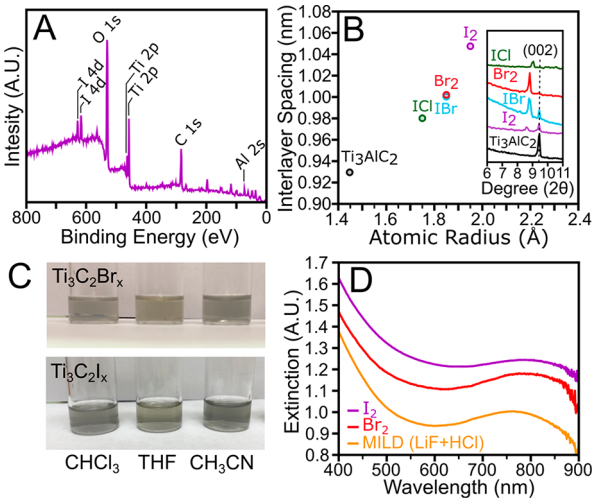

Figure 4. Halogen-etched MXenes. (A) XPS of $Ti_3C_2I_2$ from a 10 vol % I_2 in cyclohexane etch showing iodine, I 4d, signal, which indicates iodine-terminated surfaces. (B) Interlayer spacing of Ti_3AlC_2 and various halogen-terminated MXenes. Layer spacing increases with the atomic radius of halogen. (C) Photograph of stable colloidal suspensions of $Ti_3C_2Br_x$ (top) and ($Ti_3C_2I_x$ (bottom) in various low-dielectric solvents. (D) Comparison of the extinction of $Ti_3C_2I_x$ and $Ti_3C_2Br_x$ to conventional MILD etched Ti_3AlC_2 ($Ti_3C_2T_x$: T = F, OH, O) revealing a red-shift in the plasmonic resonance as the electronegativity of the surface termination decreases.

higher temperatures are required (Table S6). The etch process results in the formation of AlI_3, which may also be removed by the addition of TBAX. XPS analysis of purified flakes reveals a Ti/I composition ratio of 3:2 ($Ti_3C_2I_2$); see Figure 4A (see Section 3.0 in the Supporting Information for the complete compositional characterization). Interhalogens (*e.g.*, ICl and IBr), which dissociate more readily than molecular halogens, also etch Al from Ti_3AlC_2 (Tables S7 and S8). The unit cell expansion can be approximated *via* removal of an Al radius and addition of two halogen radii (Figure 4B, Supporting Information Section 5.0, and Table S9). For the interhalogen compounds, the more electronegative halogen atom acts as the active etching species and terminates the surface (Figure 4B). Overall these halogenated MXenes readily form stable colloidal suspensions in low dielectric organic solvents, including tetrahydrofuran (THF), acetonitrile, and chloroform; see Figure 4C. Finally, the surface plasmon resonance[55] red shifts as the electronegativity of the surface termination decreases; see Figure 4D. This can be rationalized on the basis of the polarization of the halogen−metal bond, which scales with the electronegativity of the halogen atom (F > Cl > Br > I). This induces electron density rearrangements and structural changes that modify the plasmon.

CONCLUSION

In summary, room-temperature, surface dissociation of halogens at the A-layer of the MAX phase provides an effective, mild-solution-based method to generate MXenes with halogen-terminated surfaces. As a model system, the Ti_3AlC_2 treatment with elemental halogens results in the formation of aluminum halide and halogenated $Ti_3C_2X_n$ (X = Br, I). A consistent and selective etching profile occurs in an empirically derived stoichiometry window. The rate and extent of etching may be monitored both qualitatively and optically due to a colorimetric response, which provides direct quantitative feedback in contrast to the colorless, fluoride-based methods. The etch selectivity can be optimized based on halogen radical formation at the MAX phase surface, and reactive byproducts may be sequestered *via* addition of stabilizer salts. The resulting purified, halogenated MXenes are dispersible in common organic solvents (THF and CH_3CN). The discussed batch conditions with single-step reagent addition provide ~1% yield MXene at 1 mg/mL) due to selectivity exhibiting a parabolic dependence on halogen concentration. The proposed mechanism implies that continual halogen injection using an *in situ* halogen monitor to maintain a constant etchant concentration will provide increased yields and reaction efficiency. The dispersibility in anhydrous solvents will enable postsynthetic modification of MXene surfaces via a molecular hybridization with organic moieties such as reversible addition-fragmentation chain-transfer (RAFT) polymerization or direct SN_2-type reactions on the labile Ti−X bond. Finally, the halogen etch chemistry is likely tunable across a broad range of MAX compositions due to isostructural MAX phase bonding and the tunability of halogen selectivity via temperature, concentration, and solvent. Qualitatively we have observed similar halogen etching trends with other MAX phases (Cr_2AlC; Ti_2AlC; V_2AlC); mainly, the expansion of the interlayer spacing as well as homolysis of halogens affording aluminum halides and halogenated solvents. This implies that selective etching of MAX phases with halogens is generalizable. Overall, the flexibility provided by solvent-based halogen etching will enable exciting opportunities for widespread applications, as optical and electrical properties are a function of surface composition.

EXPERIMENTAL SECTION

Materials. All chemicals were used as received unless noted, and all solvents were stored under activated molecular sieves (3 Å) to ensure anhydrous conditions. Ti_3AlC_2 MAX powder was purchased from Kai Kai Ceramics, Ltd. Liquid bromine (Br_2), iodine (I_2), iodine monobromide (IBr), iodine monochloride (ICl), tetrabutylammonium halides (chloride, bromide, and fluoride), cyclohexane (>99%), chloroform (99%), THF (99.9%), acetonitrile (99%) CS_2 (99%), lithium fluoride, and hydrochloric acid were all purchased from Sigma-Aldrich.

Methods. *$Ti_3C_2T_x$ MXene Synthesis.* All reactions were performed in a glovebox in an inert atmosphere (H_2O 0.3 ppm; O_2 0.1 ppm) and were allowed to stir at room temperature for 8 h. Over the course of the reaction, heat evolved, and the color slowly disappeared. At the end point, the crude supernatant was a light yellow, optically clear solution under activated molecular sieves (3 Å). The Ti_3AlC_2 Max phase was mixed with all different halogens in 1:2 molar ratio (Al/X = 1:4). Note that ~1:8 ratio is used in traditional minimum intensive layer delamination (MILD) and recently reported molten salts etching methods.[2,15,27,30]

Br_2 Etch. Into a glass vial was added Ti_3AlC_2 (5 mmol; 1.0 g) in 4.5 mL of cyclohexane. Liquid bromine, Br_2 (10 mmol; 0.5 mL), was added in one portion, and the slurry was allowed to stir at room temperature for 8 h. Over the course of the reaction, heat evolved, and the deep red color slowly disappeared. At the end point, the crude supernatant was a light yellow, optically clear solution.

I_2 Etch. Into a glass vial was added Ti_3AlC_2 (5 mmol; 1 g) in 4.5 mL of cyclohexane. Solid iodine, I_2 (10 mmol; 2.5 g), was added in one portion, and the mixture was allowed to stir at 70 °C for 8 h. Over the course of the reaction, heat evolved, and the deep purple color slowly disappeared. At the end point, the crude supernatant was a light purple, optically clear solution.

ICl Etch. Into a round-bottom flask was added Ti_3AlC_2 (5 mmol; 1.0 g) in 4.5 mL of CS_2. The solution was allowed to equilibrate in a

https://dx.doi.org/10.1021/acsnano.0c08630
ACS Nano 2021, 15, 2771−2777

dry ice bath (−78 °C). After equilibration (ca. 15 min), liquid ICl (10 mmol; 0.5 mL) was added in one portion, and the mixture was allowed to stir at −78 °C for 4 h.

IBr Etch. Into a round-bottom flask was added Ti_3AlC_2 (1 mmol; 0.20 g) in 4.5 mL of CS_2. Solid IBr (2 mmol; 0.41 g) was added in one portion, and the mixture was allowed to stir at room temperature for 8 h. Over the course of the reaction, heat evolved, and the deep purple color slowly disappeared. At the end point, the crude supernatant was a light purple, optically clear solution.

MILD Method. The etchant was prepared based on a previously published protocol and will be restated here for completeness.[54] The etchant was prepared by dissolving 2.00 g (77.10 mmol) of LiF in 20.00 mL of 9.0 M HCl (180.0 mmol). Ti_3AlC_2 (2.0 g, 10.07 mmol) was gradually added over the course of 5 min, and the reaction was allowed to stir for 24 h. The mixture was then diluted to a total volume of 40 mL and centrifuged at 3500 rpm for 5 min for multiple cycles, until pH 6 was achieved. After each cycle, the acidic supernatant was discarded, and fresh deionized H_2O was added. The suspension was then hand-shaken for ∼10 s before being centrifuged at 1000 rpm for seven cycles. After each cycle, the supernatant was extracted, and fresh deionized H_2O was added to the sediment. The combined extracted supernatant was vacuum-filtered through 0.170 μm pore size filter paper and recollected in minimal deionized H_2O (∼15 mL) and used for further characterization (see Figure 4D).

Processing and Cleaning. Tetrabutylammonium bromide (TBAB) was added to the reaction mixture (0.2:1 mol/mol of MAX). The reaction mixture in cyclohexane was extracted and centrifuged at 10 000 rpm. The yellow supernatant was discarded; fresh chloroform was added and centrifuged at 10 000 rpm. The centrifugation process was repeated two more times with the addition of fresh chloroform each time, until a clear supernatant was obtained. THF was added and centrifuged at 1000 rpm to sediment unexfoliated MAX phase, $AlBr_3$, and TBA byproduct. The supernatant containing $Ti_3C_2T_x$ MXene flakes was collected and centrifuged again at 1500 rpm for 20 min. The supernatant was discarded, and the sediment containing $Ti_3C_2T_x$ MXene flakes was collected and suspended in a nonpolar solvent (*i.e.*, THF, CH_3CN) for further characterization. Note that this method was equally effective with all other tetrabutylammonium halide (chloride and fluoride) tested.

Mechanism of Br_2 Etching using FTIR. All samples were prepared as batch reactions in sealed glass vials and allowed to proceed for 8 h at room temperature. In the first glass vial, 900 μL of cyclohexane was mixed with 100 μL of Br_2 and was kept in the dark. For the second reaction, 900 μL of cyclohexane was mixed with 100 μL of Br_2 and kept under UV light (354 nm). The final reaction was performed by adding Ti_3AlC_2 (1 mmol; 200 mg) in 900 μL of cyclohexane followed by the addition of 2 mmol (100 μL) of Br_2 and stored in the dark. Note that ambient light is not a sufficient activator for radical formation, but we still ran the final reaction in the dark to prevent any possible light-induced radical formation. Figure 2B,C in the main text reveals that etching proceeds via radical generation on the surface in a way that the MAX surface acts to catalyze bromine hemolysis, which reacts with both solvent and the MAX phase.

Microscopy and Spectroscopy. XRD patterns were recorded using a Smartlab system (Rigaku) with Cu Kα radiation (λ = 0.154 18 nm). Samples were prepared by depositing 50 μL of $Ti_3C_2T_x$ on clean Si wafers and allowing them to dry under ambient conditions. UV−Vis spectra of exfoliated and cleaned samples were measured on a Cary 5000 spectrometer. Electron microscopy was performed on an aberration-corrected FEI Talos TEM at an accelerating voltage of 200 kV. The samples were prepared by spotting a copper grid with 10 μL of $Ti_3C_2T_x$ drying overnight under benchtop conditions. AFM measurements were performed on a Bruker Dimension Icon. AFM of the surface morphology was measured in tapping mode using a Dimension Icon (Bruker Corporation). Standard AFM tips (Tap300Al-G, Budget Sensors) were used that contained an aluminum reflex coating with a resonant frequency of 300 kHz and a force constant of 40 N/m. The $Ti_3C_2T_x$ samples were diluted in THF, were drop-cast on Si wafers, and allowed to dry under ambient conditions. Lateral and height profiles were obtained from AFM line scans of individual particles using NanoScope Analysis software (Bruker Corporation). XPS analysis was performed using a Kratos AXIS Ultra spectrometer at high vacuum (∼2 × 10^{-9} Torr) with a monochromated Al Kα radiaiton (1486.6 eV). $Ti_3C_2T_x$ (5 μL) was pipetted out and drop-cast onto clean Si wafers. Drop-cast samples were allowed to dry at room temperature. Survey scans were collected at 10 mA and 10 kV with the electron analyzer operating in hybrid lens mode with an aperture of ∼500 μm^2. High-resolution (HR) data were collected using an analyzer pass energy of 20 eV and a step size of 0.1 eV. All data analysis utilized the CasaXPS software package.

ASSOCIATED CONTENT

Supporting Information

The Supporting Information is available free of charge at https://pubs.acs.org/doi/10.1021/acsnano.0c08630.

Additional details on the synthesis, more extensive characterization data on XRD, mechanistic insights, and compositional and structural analysis of MXene products (i.e., microscopy, XPS) from Br_2 etching, as well as I_2 etching (PDF)

AUTHOR INFORMATION

Corresponding Author

Richard A. Vaia − *Materials and Manufacturing Directorate, Air Force Research Laboratory, Wright-Patterson AFB, Ohio 45433-7702, United States;* orcid.org/0000-0003-4589-3423; Phone: 937-785-9209; Email: richard.vaia@us.af.mil; Fax: 937-656-6327

Authors

Ali Jawaid − *Materials and Manufacturing Directorate, Air Force Research Laboratory, Wright-Patterson AFB, Ohio 45433-7702, United States; UES Inc., Beavercreek, Ohio 45432, United States*

Asra Hassan − *Materials and Manufacturing Directorate, Air Force Research Laboratory, Wright-Patterson AFB, Ohio 45433-7702, United States; Department of Chemical and Biomedical Engineering, FAMU-FSU College of Engineering, Tallahassee, Florida 32310, United States*

Gregory Neher − *Materials and Manufacturing Directorate, Air Force Research Laboratory, Wright-Patterson AFB, Ohio 45433-7702, United States; Universal Technology Corporation, Beavercreek, Ohio 45432, United States*

Dhriti Nepal − *Materials and Manufacturing Directorate, Air Force Research Laboratory, Wright-Patterson AFB, Ohio 45433-7702, United States*

Ruth Pachter − *Materials and Manufacturing Directorate, Air Force Research Laboratory, Wright-Patterson AFB, Ohio 45433-7702, United States;* orcid.org/0000-0003-3790-4153

W. Joshua Kennedy − *Materials and Manufacturing Directorate, Air Force Research Laboratory, Wright-Patterson AFB, Ohio 45433-7702, United States*

Subramanian Ramakrishnan − *Department of Chemical and Biomedical Engineering, FAMU-FSU College of Engineering, Tallahassee, Florida 32310, United States*

Complete contact information is available at: https://pubs.acs.org/10.1021/acsnano.0c08630

Author Contributions

[⊥]A.J. and A.H. contributed equally to this work. All authors have given approval to the final version of the manuscript.

https://dx.doi.org/10.1021/acsnano.0c08630
ACS Nano 2021, 15, 2771−2777

Notes

The authors declare no competing financial interest.

ACKNOWLEDGMENTS

The authors acknowledge financial support by the Air Force Office of Scientific Research and the Air Force Research Laboratory's Materials and Manufacturing Directorate. A.H. and S.R. acknowledge funding from the National Science Foundation CREST center Award No. 1735968 for the current work. The authors are also appreciative of discussions with L. Beagle, D. Lioi, and J. Deitz.

REFERENCES

(1) Naguib, M.; Mochalin, V. N.; Barsoum, M. W.; Gogotsi, Y. 25th Anniversary Article: MXenes: A New Family of Two-Dimensional Materials. *Adv. Mater.* **2014**, *26* (7), 992−1005.

(2) Naguib, M.; Gogotsi, Y. Synthesis of Two-Dimensional Materials by Selective Extraction. *Acc. Chem. Res.* **2015**, *48* (1), 128−135.

(3) Nepal, D.; Kennedy, W. J.; Pachter, R.; Vaia, R. A. Toward Architected Nanocomposites: MXenes and Beyond. *ACS Nano* **2020**, DOI: 10.1021/acsnano.0c09834.

(4) Naguib, M.; Kurtoglu, M.; Presser, V.; Lu, J.; Niu, J.; Heon, M.; Hultman, L.; Gogotsi, Y.; Barsoum, M. W. Two-Dimensional Nanocrystals Produced by Exfoliation of Ti_3AlC_2. *Adv. Mater.* **2011**, *23* (37), 4248−4253.

(5) Anasori, B.; Lukatskaya, M. R.; Gogotsi, Y. 2D Metal Carbides and Nitrides (MXenes) for Energy Storage. *Nat. Rev. Mater.* **2017**, *2* (2), 16098.

(6) Deysher, G.; Shuck, C. E.; Hantanasirisakul, K.; Frey, N. C.; Foucher, A. C.; Maleski, K.; Sarycheva, A.; Shenoy, V. B.; Stach, E. A.; Anasori, B.; Gogotsi, Y. Synthesis of Mo4VAlC4MAX Phase and Two-Dimensional Mo4VC4MXene with Five Atomic Layers of Transition Metals. *ACS Nano* **2020**, *14* (1), 204−217.

(7) Srivastava, P.; Mishra, A.; Mizuseki, H.; Lee, K.-R.; Singh, A. K. *ACS Appl. Mater. Interfaces* **2016**, *8* (36), 24256−24264.

(8) Datta, D.; Li, J.; Shenoy, V. B. Defective Graphene as a High-Capacity Anode Material for Na- and Ca-Ion Batteries. *ACS Appl. Mater. Interfaces* **2014**, *6* (3), 1788−1795.

(9) Li, H.; Hou, Y.; Wang, F.; Lohe, M. R.; Zhuang, X.; Niu, L.; Feng, X. Flexible All-Solid-State Supercapacitors with High Volumetric Capacitances Boosted by Solution Processable MXene and Electrochemically Exfoliated Graphene. *Adv. Energy Mater.* **2017**, *7* (4), 1601847.

(10) Hantanasirisakul, K.; Zhao, M.-Q.; Urbankowski, P.; Halim, J.; Anasori, B.; Kota, S.; Ren, C. E.; Barsoum, M. W.; Gogotsi, Y. Fabrication of $Ti_3C_2T_x$ MXene Transparent Thin Films with Tunable Optoelectronic Properties. *Adv. Electron. Mater.* **2016**, *2* (6), 1600050.

(11) Ghidiu, M.; Lukatskaya, M. R.; Zhao, M.-Q.; Gogotsi, Y.; Barsoum, M. W. Conductive Two-Dimensional Titanium Carbide 'Clay' with High Volumetric Capacitance. *Nature* **2014**, *516* (7529), 78−81.

(12) Ran, J.; Gao, G.; Li, F.-T.; Ma, T.-Y.; Du, A.; Qiao, S.-Z. Ti_3C_2 MXene Co-Catalyst on Metal Sulfide Photo-Absorbers for Enhanced Visible-Light Photocatalytic Hydrogen Production. *Nat. Commun.* **2017**, *8* (1), 13907.

(13) Ghidiu, M.; Lukatskaya, M. R.; Zhao, M.-Q.; Gogotsi, Y.; Barsoum, M. W. *Nature* **2014**, *516* (7529), 78−81.

(14) Halim, J.; Lukatskaya, M. R.; Cook, K. M.; Lu, J.; Smith, C. R.; Näslund, L.-Å.; May, S. J.; Hultman, L.; Gogotsi, Y.; Eklund, P.; Barsoum, M. W. Transparent Conductive Two-Dimensional Titanium Carbide Epitaxial Thin Films. *Chem. Mater.* **2014**, *26* (7), 2374−2381.

(15) Alhabeb, M.; Maleski, K.; Anasori, B.; Lelyukh, P.; Clark, L.; Sin, S.; Gogotsi, Y. Guidelines for Synthesis and Processing of Two-Dimensional Titanium Carbide ($Ti_3C_2T_x$ MXene). *Chem. Mater.* **2017**, *29* (18), 7633−7644.

(16) Alhabeb, M.; Maleski, K.; Mathis, T. S.; Sarycheva, A.; Hatter, C. B.; Uzun, S.; Levitt, A.; Gogotsi, Y. Selective Etching of Silicon from Ti_3SiC_2 (MAX) To Obtain 2D Titanium Carbide (MXene). *Angew. Chem., Int. Ed.* **2018**, *57* (19), 5444−5448.

(17) Urbankowski, P.; Anasori, B.; Makaryan, T.; Er, D.; Kota, S.; Walsh, P. L.; Zhao, M.; Shenoy, V. B.; Barsoum, M. W.; Gogotsi, Y. Synthesis of Two-Dimensional Titanium Nitride Ti_4N_3 (MXene). *Nanoscale* **2016**, *8* (22), 11385−11391.

(18) Karlsson, L. H.; Birch, J.; Halim, J.; Barsoum, M. W.; Persson, P. O. Å. Atomically Resolved Structural and Chemical Investigation of Single MXene Sheets. *Nano Lett.* **2015**, *15* (8), 4955−4960.

(19) Liu, F.; Zhou, A.; Chen, J.; Jia, J.; Zhou, W.; Wang, L.; Hu, Q. Preparation of Ti_3C_2 and Ti_2C MXenes by Fluoride Salts Etching and Methane Adsorptive Properties. *Appl. Surf. Sci.* **2017**, *416*, 781−789.

(20) Peng, C.; Wei, P.; Chen, X.; Zhang, Y.; Zhu, F.; Cao, Y.; Wang, H.; Yu, H.; Peng, F. A Hydrothermal Etching Route to Synthesis of 2D MXene (Ti_3C_2, Nb_2C): Enhanced Exfoliation and Improved Adsorption Performance. *Ceram. Int.* **2018**, *44* (15), 18886−18893.

(21) Lukatskaya, M. R.; Bak, S.-M.; Yu, X.; Yang, X.-Q.; Barsoum, M. W.; Gogotsi, Y. Probing the Mechanism of High Capacitance in 2D Titanium Carbide Using *in Situ* X-Ray Absorption Spectroscopy. *Adv. Energy Mater.* **2015**, *5* (15), 1500589.

(22) Khazaei, M.; Mishra, A.; Venkataramanan, N. S.; Singh, A. K.; Yunoki, S. Recent Advances in MXenes: From Fundamentals to Applications. *Curr. Opin. Solid State Mater. Sci.* **2019**, *23* (3), 164−178.

(23) Tang, Q.; Zhou, Z.; Shen, P. Are MXenes Promising Anode Materials for Li Ion Batteries? Computational Studies on Electronic Properties and Li Storage Capability of Ti_3C_2 and $Ti_3C_2 \times 2$ (X = F, OH) Monolayer. *J. Am. Chem. Soc.* **2012**, *134* (40), 16909−16916.

(24) Hu, Q.; Sun, D.; Wu, Q.; Wang, H.; Wang, L.; Liu, B.; Zhou, A.; He, J. MXene: A New Family of Promising Hydrogen Storage Medium. *J. Phys. Chem. A* **2013**, *117* (51), 14253−14260.

(25) Halim, J.; Lukatskaya, M. R.; Cook, K. M.; Lu, J.; Smith, C. R.; Näslund, L.-Å.; May, S. J.; Hultman, L.; Gogotsi, Y.; Eklund, P.; Barsoum, M. W. Transparent Conductive Two-Dimensional Titanium Carbide Epitaxial Thin Films. *Chem. Mater.* **2014**, *26* (7), 2374−2381.

(26) Mauchamp, V.; Bugnet, M.; Bellido, E. P.; Botton, G. A.; Moreau, P.; Magne, D.; Naguib, M.; Cabioc'h, T.; Barsoum, M. W. Enhanced and Tunable Surface Plasmons in Two-Dimensional Ti_3C_2 Stacks: Electronic Structure *versus* Boundary Effects. *Phys. Rev. B: Condens. Matter Mater. Phys.* **2014**, *89*, 235428.

(27) Li, M.; Lu, J.; Luo, K.; Li, Y.; Chang, K.; Chen, K.; Zhou, J.; Rosen, J.; Hultman, L.; Eklund, P.; Persson, P. O. Å.; Du, S.; Chai, Z.; Huang, Z.; Huang, Q. Element Replacement Approach by Reaction with Lewis Acidic Molten Salts to Synthesize Nanolaminated MAX Phases and MXenes. *J. Am. Chem. Soc.* **2019**, *141* (11), 4730−4737.

(28) Li, M.; Li, X.; Qin, G.; Luo, K.; Lu, J.; Li, Y.; Liang, G.; Huang, Z.; Hultman, L.; Persson, O. Å.; Du, S.; Chai, Z.; Zhi, C.; Huang, Q. Halogenated MXenes with Electrochemically Active Terminals for High Performance Zinc Ion Batteries. *ACS Nano* Article ASAP, DOI: 10.1021/acsnano.0c07972.

(29) Jawaid, A.; Hassan, A.; Vaia, R. Preparation of Layered MXene via Elemental Halogen Etching of Max Phase. Provisional patent application number 62/934025, 2019.

(30) Kamysbayev, V.; Filatov, A.; Hu, H.; Rui, X.; Lagunas, F.; Wang, D.; Klie, R.; Talapin, D. Covalent Surface Modifications and Superconductivity of Two-Dimensional Metal Carbide MXenes. *Science* **2020**, *369* (6506), 979−983.

(31) Ehrlich, D. J.; Osgood, R. M.; Deutsch, T. F. Laser Chemical Technique for Rapid Direct Writing of Surface Relief in Silicon. *Appl. Phys. Lett.* **1981**, *38* (12), 1018−1020.

(32) Schaible, P. M.; Metzger, W. C.; Anderson, J. P. Reactive Ion Etching of Aluminum and Aluminum Alloys in an RF Plasma Containing Halogen Species. *J. Vac. Sci. Technol.* **1978**, *15* (2), 334−337.

(33) Frank, W. Method for Anisotropic Dry Etching of Metallization Layers, Containing Aluminum or Aluminum Alloys in Integrated Semiconductor Circuits, 1992, US5277750A.

(34) Harvilchuck, J. M.; Logan, J. S.; Metzger, W. C.M.; Schaible, P. Reactive Ion Etching of Aluminum, 1976, US3994793A.

(35) Pankajkumar, I.; Trived, M.; Louis, S.; Assignee, M. Production of Stabilized Aluminum Bromide Solutions, 1972, US3666686A.
(36) Glasebrook, A. L.; Lovell, W. G. The Isomerization of Cyclohexane and Methylcyclopentane. *J. Am. Chem. Soc.* **1939**, *61* (7), 1717−1720.
(37) Stevenson, D. P.; Beeck, O. The Isomerization of Cyclohexane and Methylcyclopentane in the Presence of Aluminum Halides. I. The Nature of the Catalyst. *J. Am. Chem. Soc.* **1948**, *70* (9), 2890−2894.
(38) Dunne, T. G.; Gregory, N. W. Vapor Pressures of Aluminum Chloride, Aluminum Bromide and the Mixed Halide Phase $Al_2Br_2Cl_4$. *J. Am. Chem. Soc.* **1958**, *80* (7), 1526−1530.
(39) Viola, J. T.; Seegmiller, D. W.; Fannin, A. A.; King, L. A. Vapor Pressure of Aluminum Chloride Systems. 1. Vapor Pressure and Triple Point of Pure Aluminum Chloride. *J. Chem. Eng. Data* **1977**, *22* (4), 367−370.
(40) Frank, W. E. Approaches for Patterning of Aluminum. *Microelectron. Eng.* **1997**, *33* (1−4), 85−100.
(41) Frank, W. Method for Anisotropic Dry Etching of Metallization Layers, Containing Aluminum or Aluminum Alloys in Integrated Semiconductor Circuits, 1999, US5277750A.
(42) Schmidt, V. A.; Quinn, R. K.; Brusoe, A. T.; Alexanian, E. J. Site-Selective Aliphatic C-H Bromination Using N -Bromoamides and Visible Light. *J. Am. Chem. Soc.* **2014**, *136* (41), 14389−14392.
(43) Shaw, H.; Perlmutter, H. D.; Gu, C.; Arco, S. D.; Quibuyen, T. O. Free-Radical Bromination of Selected Organic Compounds in Water. *J. Org. Chem.* **1997**, *62* (2), 236−237.
(44) Jones, F.; Tran, H.; Lindberg, D.; Zhao, L.; Hupa, M. Thermal Stability of Zinc Compounds. *Energy Fuels* **2013**, *27* (10), 5663−5669.
(45) Nakayama, K.; Aldao, C. M.; Weaver, J. H. Halogen Etching of Si(100)-2 × 1: Dependence on Surface Concentration. *Phys. Rev. B: Condens. Matter Mater. Phys.* **1999**, *59* (24), 15893−15901.
(46) Nakayama, K.; Aldao, C. M.; Weaver, J. H. Vacancy-Assisted Halogen Reactions on Si(100)- (2 × 1). *Phys. Rev. Lett.* **1999**, *82* (3), 568−571.
(47) Presser, V.; Heon, M.; Gogotsi, Y. Carbide-Derived Carbons - From Porous Networks to Nanotubes and Graphene. *Adv. Funct. Mater.* **2011**, *21* (5), 810−833.
(48) Schaible, P. M.; Metzger, W. C.; Anderson, J. P. Reactive Ion Etching of Aluminum and Aluminum Alloys in an RF Plasma Containing Halogen Species. *J. Vac. Sci. Technol.* **1978**, *15* (2), 334−337.
(49) Tokunaga, K.; Redeker, F. C.; Danner, D. A.; Hess, D. W. Comparison of Aluminum Etch Rates in Carbon Tetrachloride and Boron Trichloride Plasmas. *J. Electrochem. Soc.* **1981**, *128* (4), 851−855.
(50) Scholz, F.; Himmel, D.; Eisele, L.; Unkrig, W.; Martens, A.; Schlüter, P.; Krossing, I. The Acidity of the $HBr/AlBr_3$ System: Stabilization of Crystalline Protonated Arenes and Their Acidity in Bromoaluminate Ionic Liquids. *Chem. - Eur. J.* **2015**, *21* (20), 7489−7502.
(51) Corma, A.; García, H. Lewis Acids: From Conventional Homogeneous to Green Homogeneous and Heterogeneous Catalysis. *Chem. Rev.* **2003**, *103* (11), 4307−4365.
(52) Lipatov, A.; Alhabeb, M.; Lukatskaya, M. R.; Boson, A.; Gogotsi, Y.; Sinitskii, A. Effect of Synthesis on Quality, Electronic Properties and Environmental Stability of Individual Monolayer Ti_3C_2 MXene Flakes. *Adv. Electron. Mater.* **2016**, *2* (12), 1600255.
(53) Novoselov, K. S.; Jiang, D.; Schedin, F.; Booth, T. J.; Khotkevich, V. V.; Morozov, S. V.; Geim, A. K. Two-Dimensional Atomic Crystals. *Proc. Natl. Acad. Sci. U. S. A.* **2005**, *102* (30), 10451−10453.
(54) Coy Diaz, H.; Addou, R.; Batzill, M. Interface Properties of CVD Grown Graphene Transferred onto MoS 2(0001). *Nanoscale* **2014**, *6* (2), 1071−1078.
(55) El-Demellawi, J. K.; Lopatin, S.; Yin, J.; Mohammed, O. F.; Alshareef, H. N. Tunable Multipolar Surface Plasmons in 2D $Ti_3C_2T_x$ MXene Flakes. *ACS Nano* **2018**, *12* (8), 8485−8493.

https://dx.doi.org/10.1021/acsnano.0c08630
ACS Nano 2021, 15, 2771−2777